

## Article

# Micromechanism of Cold Deformation of Two Phase Polycrystalline Ti-Al Alloy with Void Defect

**Author** 

- <sup>1</sup> School of Mechanical and Electronical Engineering, Lanzhou University of Technology, Lanzhou 730050, China;  
<sup>2</sup> State Key Laboratory of Advanced Processing and Recycling of Non-ferrous Metals, Lanzhou University of Technology, Lanzhou 730050, China  
\* Correspondence: e-mail@e-mail.com; Tel.: +x-xxx-xxx-xxxx

Version November 22, 2018 submitted to Journal Not Specified

**Abstract:** Cold deformation behavior of poly crystalline metallic material is affected by intrinsic defects such as dislocation, etc. Existing studies on  $\alpha_2(\text{Ti}_3\text{Al})+\gamma(\text{TiAl})$  two phase Ti-Al alloy covers about deformation behavior mainly on macro scale. This paper focus on the cold deformation mechanism of two phase Ti-Al alloy at micro scale, and the role of void defect in deformation process. Molecular dynamics simulations were performed to study the evolution of micro structure in the material under uniaxial tension. Interaction between spherical nano void with different size and position was also examined in the simulation. The results show that (1)  $\gamma$  phase is the major deformation source of the two phase alloy; (2) Void defect detracts the strength of the two phase alloy, however the position of void affect the degree of this subtraction, voids located at the  $\alpha_2/\gamma$  phase boundary have significant detraction to strength.

**Keywords:** two phase Ti-Al alloy, void, molecular dynamics, cold deformation

## 1. Introduction

Titanium aluminum based intermetallic alloys are promising high temperature structural materials because of their great corrosion resistance and strength at high temperature. Comparing with nickel based alloy, Ti-Al based alloys have lower density and are prone to be utilized in combustion engine, turbine, and other components work at high temperature ranging from 500 °C to 900 °C [1]. The performance of inner combustion engine with components made of Ti-6Al-4V was improved 20% because the weight of components decreased from 30% to 40% [2]. With the advancement of non-ferrous metallurgy, Ti-Al based alloy components has better economic efficiency than ever before. Ti-Al based alloys have good prospects for applications in aerospace and automobile industry. Poor ductility of Ti-Al alloy at room temperature strongly affects the safety of structures like turbo of aircraft engine and combustion generator [3]. Deformation phenomena of Ti-Al alloys have been widely studied in order to overcome the problems associated with the limited ductility and damage tolerance. Much of the work has been performed on single phase  $\gamma$ -TiAl alloys and polysynthetically twinned crystals(PTC)[4]. Rapture failure at the macroscopic scale can be attributed to abrupt nucleation, growth and propagation of cracks, but at the microscopic scale defects are initially easily formed in the casting process, such as voids and inclusions [5]. A great number of literatures cover a wide range of factors such as alloy composition, microstructure and deformation temperature,some reports come up with idea that two phase titanium aluminum alloys with proper phase distribution and grain size exhibit better mechanical performance compared with monolithic constituents  $\gamma(\text{TiAl})$  and  $\alpha_2(\text{Ti}_3\text{Al})$  alloy [6]. Void defect can arise due to specific volume differences induced by precipitation or by different thermal expansion or shrinkage upon heating or cooling the specimen. It has been known that

nucleation, growth and coalescence of voids are deemed as the primary mechanism of ductile material fracture, in which void growth is particularly important [7]. The initiation of crack at microscopic scale is a dynamic process, which resulting in difficulties on study about mechanisms of deformation and cracking, these defects are known to play a fundamental role in the deformation of materials. Multiscale method have been applied to study deformation behavior of polycrystal with single aluminum [8] and titanium element respectively [9]. It's necessary to carefully examine the revolution of defects and its influence on the fracture process at atomic scale. The effect of void defect is another great concern about properties and deformation mechanism of TiAl alloy. Therefore, it is necessary to study the deformation response of intermetallics structural materials with the consideration of microstructure evolution. Previous study on void growth in single crystal  $\gamma$ -TiAl reveals that void with high volume fraction detracts yield strength, and emission of dislocation [5,10]. Evolution of void in ductile polycrystalline was studied in nanoscale with molecular dynamics(MD) simulations, [11,12], voids inside material are sources of dislocation and affects the properties of materials differently because of difference in size and position. The deformation and fracture mechanisms in the duplex microstructure are plasticity induced grain boundary decohesion and cleavage, while those in the lamellar micro-structure are interface delamination and cracking across the lamellar [5]. It reveals that existence of voids alone may contribute to strain hardening because they are barriers to dislocation movement in ductile fcc structure metal[13]. However, few literature covers about deformation mechanism of two phase Ti-Al alloy and the role of void in atomic scale. Defects are inevitable as micro-pores and loosen from casting, and in the actual work environment with radiation. A lot of work carried out on the effect of various defects on the behavior of different materials, show that point defects may affect the properties of materials greatly. The mechanical performance of irradiated copper is affected by the interaction between irradiation and dislocation [14]. Vacancy concentration in single crystal and polycrystal Fe–40 at. Al bulk results in an increase of strength [15]. Ti-Al alloy is a type of typical brittle material, thus it can be assumed that its properties are sensitive to the existence of void defect. Surface defects such as small notches can cause low and high cycle fatigue strength of the Ti–47Al–2W–0.5Si alloy [16], and the strength of single crystal  $\gamma$ -TiAl is also lowered by point defect [17]. The resistance of Ti–6Al–4V alloy, which was processed for typical fan blade applications, to high-cycle fatigue in the presence of foreign- object damage was markedly reduced due to earlier crack initiation. The nucleation and subsequent near-threshold growth of crack was primarily affected by the stress concentration associated with the foreign-object damage and the presence of small micro-cracks in the damaged zone. Due to difficulties in observing the dynamic process during deformation with experiments, MD simulation has become an effective method to investigate micro deformation mechanism. Defects such as grain boundary, void and segregation play a significant role in the process of fracture [18]. This paper focus on the evolution of microstructure, tend to find out its connection to cold deformation behavior of two phase TiAl alloy. MD simulation including model creation and analysis method is given in Section 2, Results and discussion are in Section 3.

## 2. Molecular Dynamics Simulation

### 2.1. Atomic Potential

The interaction of particle in the material is determined by interatomic potential. Many reported simulation cases of deform and crack propagation in metal materials were performed with embedded atomic method due to its better accuracy in metal lattice compare with F-S and L/J [19–21]. Embedded atom method (MEAM) potential developed by Zope and Mishin [22] was used in the study. The simulation is submitted by MD simulations with the Large-scale Atomic/Molecular Massively Parallel Simulator (LAMMPS) open-source code [23]. We performed constant-pressure and constant-temperature (NPT) molecular dynamics simulation at room temperature (298K). The definition of potential is as following:

$$E_{total} = \sum F_i(\rho_{h,i}) + \frac{1}{2} \sum_i \sum_{j \neq i} \phi_{ij}(R_{ij}) \quad (1)$$

where  $E_{total}$  is the total energy of the system,  $\rho_{h,i}$ , is the host electron density at atom  $i$  due to the remaining atoms of the system,  $F_i(\rho)$  represents the energy for embedding atom  $i$  into the background electron density  $\rho$ , and  $\phi_{ij}(R_{ij})$  gives the core-core pair repulsion between atoms  $i$  and  $j$  separated by the distance  $R_{ij}$ . It can be noted that  $F_i$  only depends on the element of atom  $i$  and  $\phi_{ij}$  only depends on the elements of atoms  $i$  and  $j$ .

## 2.2. Model Creation of Crystalline

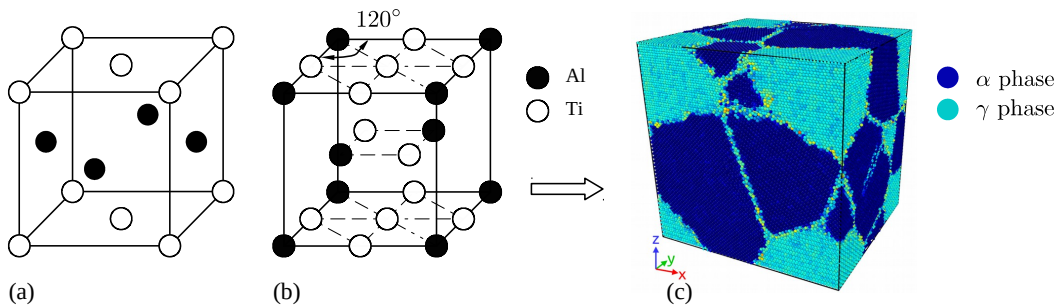


**Figure 1.** Unit cell of TiAl (a),  $Ti_3Al$  (b) and two phase Ti-Al model (c)

**Table 1.** Parameters of nanocrystalline

Phase	Space group	Designation	Parameters
$\alpha_2 - Ti_3Al$	P6 <sub>3</sub> /mmc	0 <sub>19</sub>	$a = 0.5765$ $c = 0.46833$
$\gamma - TiAl$	tP4	L1 <sub>0</sub>	$a = 0.3997$ $c = 0.4062$

Two phase Ti-Al alloy is composed of  $\gamma$ -TiAl and  $\alpha_2$ - $Ti_3Al$  has a fcc type cell with an  $L1_0$  structure, and  $\alpha_2$ - $Ti_3Al$  has a hcp structure, these two types of initial cells are shown in Fig. 1, constructing parameters of the two type of unit cell are given by table 1. Periodic boundary conditions (PBC) are applied along all three directions, that makes polycrystal with periodic nanovoid structures. The initial dimension of simulation cell is  $L_x = 200 \text{ \AA}$ ,  $L_y = 180 \text{ \AA}$ ,  $L_z = 210 \text{ \AA}$ , and each model contains about 460,000 atoms. The grain orientation and size were randomly created with Voronoi method by code ATOMSK [24], and resulting in the arbitrary shape and orientation of the grains. Uniaxial load was applied to the model at a strain rate of  $5 \times 10^8 \text{ s}^{-1}$ .

## 2.3. Analysis method

In order to identify typical defects in the deformed model, a hybrid analysis method was used with free code ovito[25]. Dislocation is visualized by DXA method, and Centro-symmetry parameter(CSP) is used to tell grain boundary from  $\alpha_2$  phase and  $\gamma$  phase. The definition of CSP is as following:

$$P = \sum_{i=1}^6 |\vec{R}_i + \vec{R}_{i+6}|^2 \quad (2)$$

where  $\vec{R}_i$  and  $\vec{R}_{i+6}$  are the vectors corresponding to the six pairs of opposite nearest neighbors in the fcc lattice. The centro-symmetry parameter(CSP) is zero for atoms in a perfect lattice. In other words, if the lattice is distorted, the value of P will not be zero. Instead, the parameter will have a

value within the range corresponding to a particular defect. By removing all the perfect and surface atoms within the bulk, atoms around defected zone are visualized.

### 3. Results and Discussion

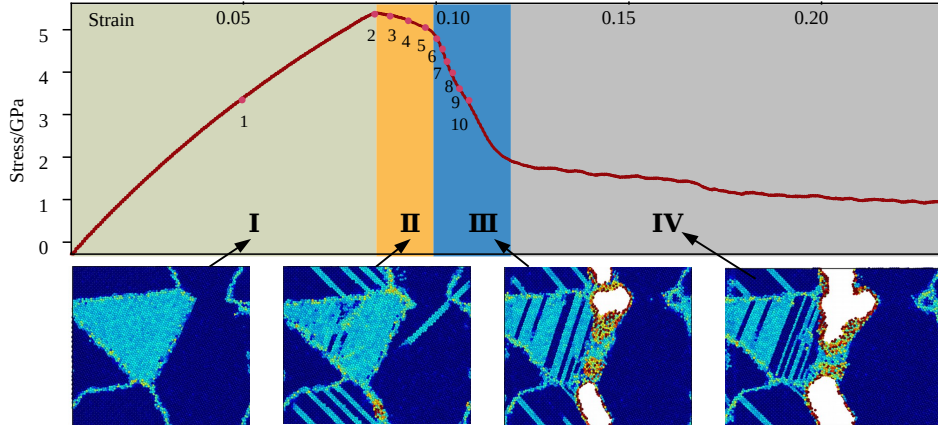


**Figure 2.** Deformation process of the model without void defect

Deformation process of the model without void defect is shown in Fig. 2. The strength of the model without void defect is 5.3 GPa. According to stress response under constant rate of strain rate, the whole tensile process can be divided into four stages: stage - I: elastic stage, ranging from  $\epsilon = 0$  to  $\epsilon = 0.092$ , including key point 1, stage - II: yield stage, ranging from  $\epsilon = 0.092$  to  $\epsilon = 0.101$ , including key points 2 to 6, stage - III: cracking stage, ranging from  $\epsilon = 0.101$  to  $\epsilon = 0.112$ , including key point 7 to 10, stage - IV: fracture stage. Following discussion concentrates on deformation phenomena that rely on the elasto-plastic codeformation of the  $\gamma$  and  $\alpha_2$  phases and on the particular point defect situation occurring in two phase alloys.

**Table 2.** Key points during tensile process

Number	1	2	3	4	5	6	7	8	9	10
Stage	I	I	II	II	II	II	III	III	III	III
Strain	0.05	0.088	0.092	0.096	0.099	0.101	0.104	0.107	0.110	0.112

#### 3.1. Deformation Mechanism of Two Phase TiAl Alloy without Void Defects

Snapshots of atom configuration at the 3 of 10 key points are shown by Fig. 3. Atoms with ordered configuration of  $\gamma$  phase grains have been removed in Fig. 3(a) and (b),  $\alpha_2$  phase and defects inside grains have been left. Similarly,  $\gamma$  phase grain have been removed in Fig. 3(c) and (d), the defects of  $\alpha_2$  phase have been left. The results show that, at stage I, the structure of material is under typical elastic deformation and the size of simulation box enlarged due to the loading, deformation of the two phase are compatible. Emission of dislocation and evolution of defects initiated at the end of stage I. A great number of dislocation emitted inside  $\gamma$  phase at earlier part of stage II, however, the dislocation inside  $\alpha_2$  phase was emitted at the end of stage II shown by Fig. 3(c). Experiments have shown that the velocity of dislocation motion is sensitive to stress and temperature[28]. The brittleness of two phase Ti-Al alloy attributed to the poor mobility of dislocation at room temperature. Velocity of a screw dislocation can be estimated by Escaig's elastic model [29], it can be written as:

$$v = v_0 e^{-\Delta H(\tau^*)/kT} \quad (3)$$

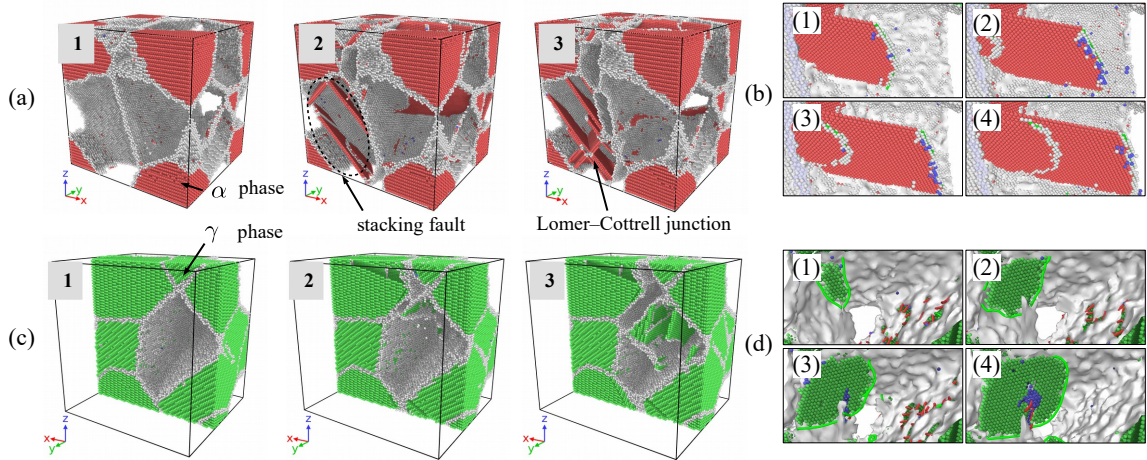


**Figure 3.** Microstructure evolution inside  $\gamma$  phase(a,b),  $\alpha_2$  phase(c,d) during yield stage

where the prefactor  $v_0$  gives the velocity that would be obtained for each potential mobility,  $L$  represents the free length of screw character of dislocation,  $\Delta H(\tau^*)$  is activation enthalpy determined by loading conditions. The effect of temperature on the mobility can be evaluated under different loading conditions, thus we chose  $\tau_1^* > \tau_2^* > \tau_3^*$  in formulation (3), normalized velocity of dislocation motion is shown by Fig. 4. The velocity of dislocation movement rise along with increase of stress, the mobility of dislocation is relatively poor at 298 K. Due to motion of dislocation is inactive inside  $\alpha_2$  phase, piling up of dislocations, the typical strengthening mechanism closely related with interaction between grain boundary and dislocation can not be dramatic at room temperature. That is in good agreement with simulation results shown by in Fig. 3, there was few dislocation piling up at near boundaries.

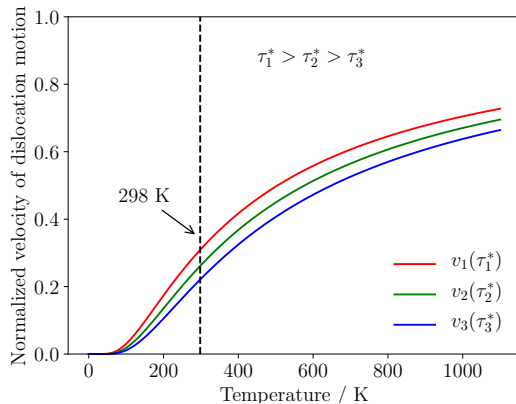


**Figure 4.** Normalized velocity of dislocation motion under different loading conditions

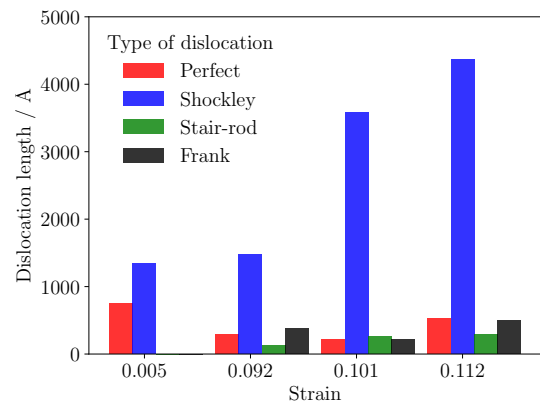
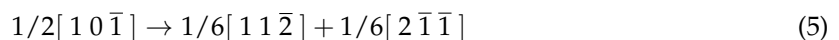
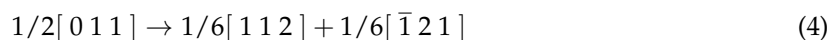
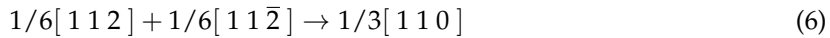


**Figure 5.** Dislocation length under different strain

Length of different types of dislocations are given at four stages in Fig. 5. Dislocations are recognized and identified using the dislocation analysis (DXA) of OVITO. The length of Shorckley dislocation with Burgers vector  $1/6[112]$  increase sharply during yield stage of the deformation process in Fig. 5, but the length of perfect dislocation fluctuate at a low level. Decomposition of the perfect dislocations split into Shockley partial dislocations as formulation (4) and (5). The structure spontaneously transform into intrinsic stacking fault (ISF), it can be observed in Fig. 3(a).



Interaction between dislocation with Burgers vector of  $1/6[112]$  and  $1/6[1\bar{1}\bar{2}]$  follows the decomposition of perfect dislocation. The process produce leading dislocation and a trailing dislocation, when the two leading Shockley partials combine, they form Lomer–Cottrell junction, a separate dislocation. It's sessile and immobile in the slip plane, plays a role of barrier against other dislocations in the plane. This process can be given by :



According to results calculated by first principle, the stacking faulting energy for TiAl is much smaller than  $Ti_3Al$ , as a consequence calculated shear strength of TiAl and  $Ti_3Al$  is 4.1 Gpa and 2.86 Gpa along their easy slip plane respectively[27]. This calculation reveals that tensile behaviour in single crystal is mainly controlled by the type of the structure. However, in two phase Ti-Al alloy, deformation of  $\alpha_2$  phase is earlier than  $\gamma$  phase during yield stage, thus local displacement of two phases are incompatible during yield stage. Mobility of dislocation is affected by structure of crystal, loading condition and temperature.  $\alpha_2$  phase is made up of hcp structured grain, grain with this type of structure possess less slip system comparing with grain with fcc structure [26], thus  $\alpha_2$  phase is difficult to be deformed under uniaxial tensile loading.

Main reason for the unequal strain partitioning between the  $\alpha_2$  and  $\gamma$  phase is certainly the strong plastic anisotropy of the  $\alpha_2$  phase. TEM examinations performed on tensile tested lamellar alloys have revealed that the limited plasticity of the  $\alpha_2$  phase is carried by local slip of  $\langle a \rangle$ -type dislocations with the Burgers vector  $b = 1/3[11\bar{2}0]$  prism planes shown by Fig. 3(b), which is by far the easiest slip system in  $\alpha_2$  single crystals. The core of a dislocation intersecting an interface often needs to be transformed. For example, an ordinary  $1/2[110]$  dislocation gliding in one  $\gamma$  grain has to be converted into a  $[101]$  super dislocation with the double Burgers vector gliding in an adjacent  $\gamma$  grain. At the  $\alpha_2/\gamma$  interface, dislocations existing in the  $D0_{19}$  structure have to be transformed into dislocations consistent with the  $L1_0$  structure. These core transformations are associated with a change of the dislocation line energy because the lengths of Burgers vectors and the shear module are different. Dislocations crossing semi-coherent boundaries have to intersect the misfit dislocation, a process that involves elastic interaction, jog formation and the incorporation of gliding dislocations into the mismatch structure of the interface. When slip is forced to cross  $\alpha_2$  phase, pyramidal slip of the  $\alpha_2$  phase is required, which needs an extremely high shear stress.

### 3.2. The effect of void on the strength of material

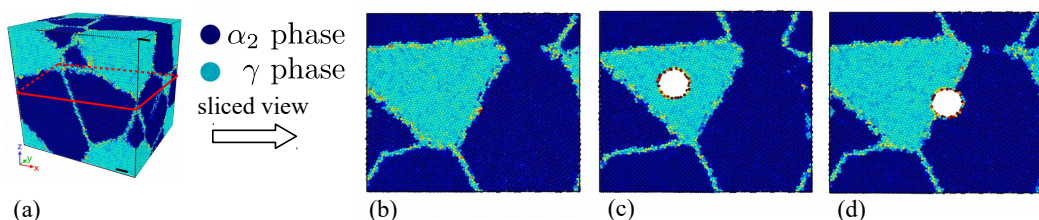


**Figure 6.** Model with no void defect (b), with void inside  $\alpha_2$  phase (c) with void at  $\alpha_2 - \gamma$  interface (d)

In Fig. 6, voids with different size: 2Å, 5Å, 10Å, 15Å were placed at  $\alpha_2/\gamma$  phase boundary, inside  $\gamma$  phase respectively. The strength of materials with void in different size and at different position is shown in Fig. 7. The existence of void have little impact on the elastic properties of the material, and the model without void defect has the best strength 5.3 GPa, the yield stress of model with void is smaller. Void at  $\alpha_2/\gamma$  phase boundary detracts the strength of material most, and the void inside  $\alpha_2$  phase have less impact on the strength. Conventional definition of strength of materials with geometry subtraction was applied to the model, and theoretical strength of the models was calculated by

$$\sigma^* = \sigma_0 \cdot (A^*/A_0) \quad (7)$$

where  $\sigma_0$  is the strength of model without void defects 5.3 Gpa, and  $A_0$  represents initial section area,  $A^*$  is effective section area in consider of the area detraction by void. In classic theory, the relationship between void size and strength of the model is linear. However, simulation results reveals that two phase Ti-Al alloy is sensitive to existence of void defect. Comparing with the strength determined by molecular dynamics simulation and the result4s calculated with formulation (7), it can be assumed that the main factor that affects the strength of materials can be attributed to local behavior of the materials, thus revolution of defects have dramatic influence on the yield and fracture process of the materials.

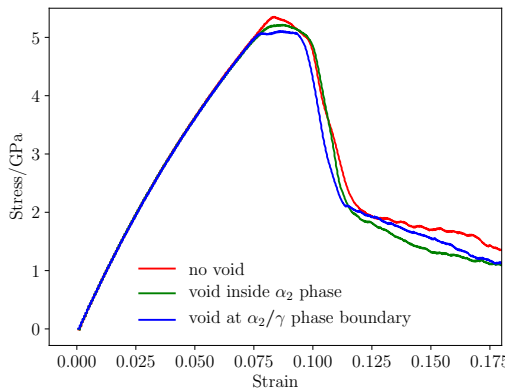


**Figure 7.** Stress-strain response of models

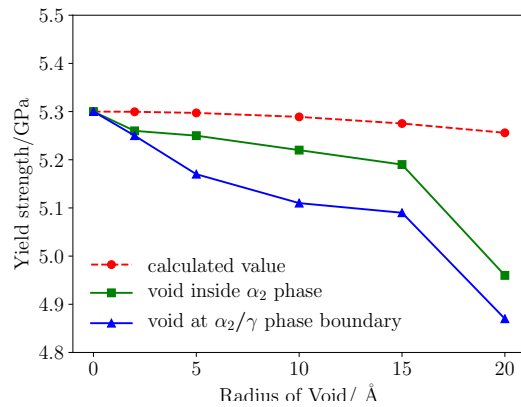


**Figure 8.** Yield strength of material with void

It has been observed in Fig. 8 that voids detracts the strengths of material. The max stress of the simulation cell decreases as the volume of voids are larger. From Fig. 7, there is a critical value of void radius about 15 Å, the void greater than 15 Å cause serious detraction of strength of material. The decrease rate of loading area are smaller comparing with the detraction of strength, so it can be assumed that the yield behavior and strength is much more related with local behavior of grain boundaries and void. Grain and phase boundaries are obstacles to deformation process, thus the stability of boundaries have great impact on the strength of materials. Interactive between grain boundary and void determines the fracture mode of the TiAl alloy.

### 3.3. Evolution of spherical void

The role of void can be concluded as two main parts: source of dislocations and obstacles to dislocations, which part is dominant depends on the location of void. Void inside  $\alpha_2$  phase plays a role of inclusion, in other words, this type of void possess similar properties as second phase particles.

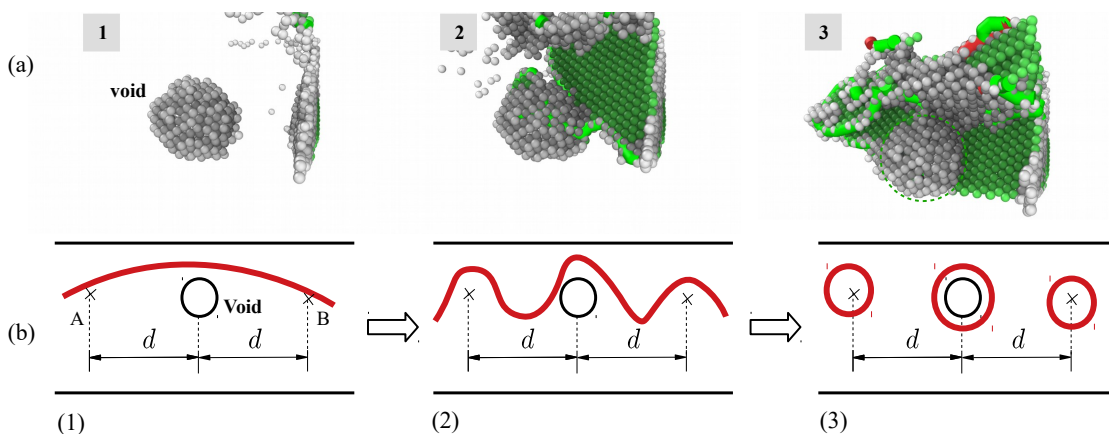


**Figure 9.** Orowan process in  $\alpha_2$ -phase (atoms with regular arrangement have been removed)

Void inside  $\alpha_2$  phase induce considerable misfit-stress fields and thus can influence material properties pronouncedly. Such stress fields surrounding the second-phase particles can be due to misfit between  $\alpha_2$  phase atoms and 'free' atoms surrounded the void. That's a possibly favorable effect of second-phase particles that void defect contribution to the enhancement of mechanical strength. The strengthening effect of the particle inside single phase TiAl alloy have been verified by experiment [31]. Considering yielding of a material as related to glide of dislocations, any mechanism obstructing dislocation glide improves the mechanical strength. The defect evolution neighboring the void during yield stage is given by Fig. 9(a), the role of void is similar to second-phase particles. It can serve as obstacles for dislocation migration which is shown by Fig. 9(b): the stress fields surrounding the second-phase particles can be of block propagation of the stress field of a migrating dislocation, the void particle acts as pinning point. The dislocation can pass two pinning points a critical shear stress is needed that depends on the distance between obstacles, which can be regarded as second-phase particles[13]:

$$\tau_0 = Gb/d \quad (8)$$

where  $d$  represents the distance between two obstacles A and B in Fig. 9 , reflects the dependence of the critical shear stress  $\tau_0$  on the second-phase particle density and distribution. This mechanism for hardening is designated as the Orowan process with  $\tau_0$  as the Orowan shear stress. As a result of the Orowan process, upon passage of the pinning points by a series of gliding dislocations, a system of concentric loops is formed around the second-phase particles. Consequently, the effective average distance between the second phase particles has decreased to  $d$  which implies a necessary increase of the value of critical shear stress required for continuation of dislocation glide. The width of a burgers vector, will be generated at both sides of a crystal along the direction of burgers vector after dislocation traversing the entire crystal, as is shown in the third sub-figure of Fig. 9(b).

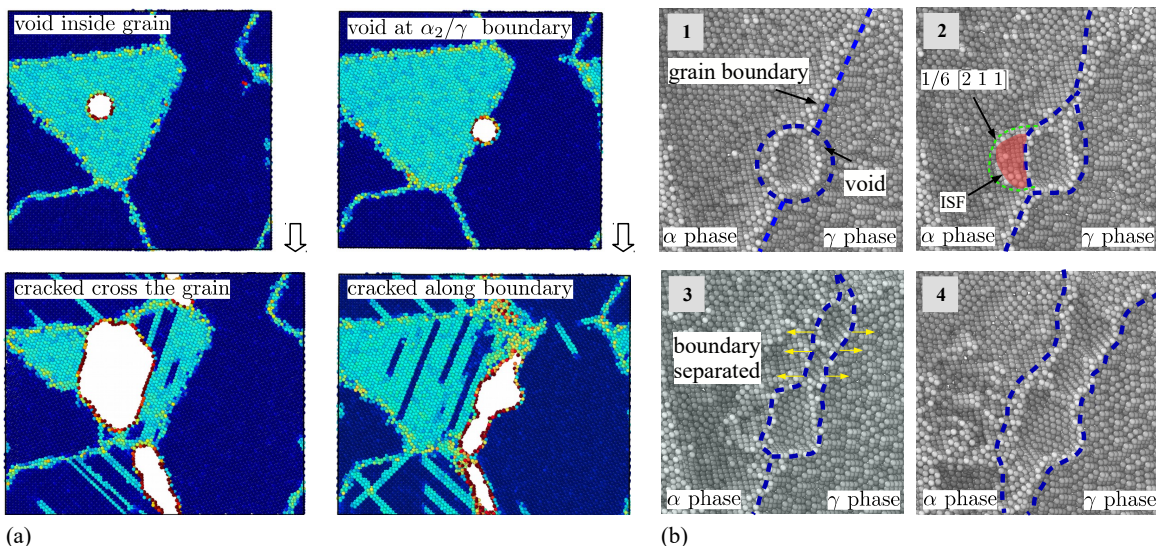


**Figure 10.** (a) Fracture mode of two types of model (b)Evolution of void at phase boundary

Effect of voids at different positions on the crack mode of the material are shown by Fig. 10(a). The model with void fractured cross the grain, and the model with void at  $\alpha_2/\gamma$  boundary resulted a large crack along the boundary under tensile loading. The difference of crack mode can attribute to the position of void and the evolution of the defect. Nucleation, emission of Shockley partial dislocation affect the evolution of the void at boundary greatly due to the anisotropy of two phases on the both sides of the phase boundary. The void weaken the strength of the grain it locates,  $\alpha_2$  phase grain is easy to deformed under shear stress, thus that caused the crack initiated inside grain and finally caused fracture across the grain. Deformation mechanism of the model with void at boundary can be more complex due to the interaction between void and phase boundary. In elastic stage, the

system composed of  $\alpha_2$  phase,  $\gamma$  phase and void is in equilibrium, internal stress are balanced under compatible deformation as is shown by the first sub-figure of Fig. 10(b). In the middle moment of yield stage, partial dislocation with Burgers vector  $1/6[\bar{2}\bar{1}1]$  emitted from surface of void in Fig. 10(b)-2. The micro crack initialed from the zone neighbor the interface between void and boundary, that quickly caused abrupt decohesion of phase boundary. That accounts for the reason that material with void at  $\alpha_2/\gamma$  phase boundary is weaker than other cases.

#### 4. conclusion

In this paper, deformation behavior of two phase Ti-Al alloy under tensile loading was simulated with MD method. The mechanism of deformation was investigated under atomic scale, and the effect of void defect on the properties of two phase Ti-Al alloy was also studied. The conclusions are as follows:

- (1) Major deformation component of the two phase TiAl alloy is  $\gamma$  phase,  $\alpha_2$  phase is harder to be deformed, this inhomogeneity results in cracks at interface of the two phase.
- (2) Effect of void defect on the strength of the two phase alloy is sensitive to the location of void. Void inside grain have less detraction to the strength of material because of strengthening mechanism similar to second phase particle. Void at  $\alpha_2/\gamma$  boundary is most risky situation for two phase alloy because of fast fracture along boundary.

#### References

1. Clemens, H.; Mayer, S. Advanced Intermetallic TiAl Alloys. *Materials Science Forum* **2016**, *879*, 113–118. doi:10.4028/www.scientific.net/MSF.879.113.
2. Bewlay, B.P.; Nag, S.; Suzuki, A.; Weimer, M.J. TiAl alloys in commercial aircraft engines. *Materials at High Temperatures* **2016**, *33*, 549–559. doi:10.1080/09603409.2016.1183068.
3. Martíková, N.; Nová, P.; Sablina, O.V.; Graphodatsky, A.S.; Zima, J. Karyotypic relationships of the Tatra vole (*Microtus taticus*). *Folia Zoologica* **2004**, *53*, 279–284, [arXiv:1011.1669v3]. doi:10.1007/s13398-014-0173-7.2.
4. Appel, F.; Clemens, H.; Fischer, F.D. Modeling concepts for intermetallic titanium aluminides. *Progress in Materials Science* **2016**, *81*, 55–124. doi:10.1016/j.pmatsci.2016.01.001.
5. Xu, X.T.; Tang, F.L.; Xue, H.T.; Yu, W.Y.; Zhu, L.; Rui, Z.Y. Molecular dynamics simulations of void shrinkage in  $\gamma$ -TiAl single crystal. *Computational Materials Science* **2015**, *107*, 58–65. doi:10.1016/j.commatsci.2015.05.007.
6. Kim, Y.W. Effects of microstructure on the deformation and fracture of  $\gamma$ -TiAl alloys. *Materials Science and Engineering A* **1995**, *192-193*, 519–533. doi:10.1016/0921-5093(94)03271-8.
7. Hempel, N.; Bunn, J.R.; Nitschke-Pagel, T.; Payzant, E.A.; Dilger, K. Study on the residual stress relaxation in girth-welded steel pipes under bending load using diffraction methods. *Materials Science and Engineering A* **2017**, *688*, 289–300. doi:10.1016/j.msea.2017.02.005.
8. Groh, S.; Marin, E.B.; Horstemeyer, M.F.; Zbib, H.M. Multiscale modeling of the plasticity in an aluminum single crystal. *International Journal of Plasticity* **2009**, *25*, 1456–1473. doi:10.1016/j.ijplas.2008.11.003.
9. Liu, X.; Sun, W.K.; Liew, K.M. Multiscale modeling of crystal plastic deformation of polycrystalline titanium at high temperatures. *Computer Methods in Applied Mechanics and Engineering* **2018**, *340*, 932–955. doi:10.1016/j.cma.2018.06.026.
10. Xu, S.Z.; Hao, Z.M.; Su, Y.Q.; Yu, Y.; Wan, Q.; Hu, W.J. An analysis on nanovoid growth in body-centered cubic single crystalline vanadium. *Computational Materials Science* **2011**, *50*, 2411–2421. doi:10.1016/j.commatsci.2011.03.019.
11. Jing, P.; Yuan, L.; Shivpuri, R.; Xu, C.; Zhang, Y.; Shan, D.; Guo, B. Evolution of spherical nanovoids within copper polycrystals during plastic straining: Atomistic investigation. *International Journal of Plasticity* **2018**, *100*, 122–141. doi:10.1016/j.ijplas.2017.09.016.
12. Elkhatib, M.G.; Shin, Y.C. Molecular dynamics-based cohesive zone representation of Ti6Al4V/TiC composite interface. *Materials and Design* **2018**, *155*, 161–169. doi:10.1016/j.matdes.2018.05.054.

13. Xiong, L.; Xu, S.; McDowell, D.L.; Chen, Y. Concurrent atomistic-continuum simulations of dislocation-void interactions in fcc crystals. *International Journal of Plasticity* **2015**, *65*, 33–42. doi:10.1016/j.ijplas.2014.08.002.
14. Kiener, D.; Hosemann, P.; Maloy, S.A.; Minor, A.M. In situ nanocompression testing of irradiated copper. *Nature Materials* **2011**, *10*, 608–613. doi:10.1038/nmat3055.
15. Yang, Y.; Baker, I. The influence of vacancy concentration on the mechanical behavior of Fe-40Al. *Intermetallics* **1998**, *6*, 167–175. doi:10.1016/S0966-9795(97)00062-9.
16. Nazmy, M.; Staubli, M.; Onofrio, G.; Lupinc, V. Surface defect tolerance of a cast TiAl alloy in fatigue. *Scripta Materialia* **2001**, *45*, 787–792. doi:10.1016/S1359-6462(01)01097-1.
17. Wu, H.N.; Xu, D.S.; Wang, H.; Yang, R. Molecular Dynamics Simulation of Tensile Deformation and Fracture of  $\gamma$ -TiAl with and without Surface Defects. *Journal of Materials Science and Technology* **2016**, *32*, 1033–1042. doi:10.1016/j.jmst.2015.12.001.
18. Larsen, P.M.; Schmidt, S.; SchiØtz, J. Robust structural identification via polyhedral template matching. *Modelling and Simulation in Materials Science and Engineering* **2016**, *24*, 055007, [1603.05143]. doi:10.1088/0965-0393/24/5/055007.
19. Ko, W.S.; Grabowski, B.; Neugebauer, J. Development and application of a Ni-Ti interatomic potential with high predictive accuracy of the martensitic phase transition. *Physical Review B - Condensed Matter and Materials Physics* **2015**, *92*, 134107. doi:10.1103/PhysRevB.92.134107.
20. Zepeda-Ruiz, L.A.; Stukowski, A.; Oppelstrup, T.; Bulatov, V.V. Probing the limits of metal plasticity with molecular dynamics simulations. *Nature* **2017**, *550*, 492–495. doi:10.1038/nature23472.
21. Fan, H.; Zhu, Y.; El-Awady, J.A.; Raabe, D. Precipitation hardening effects on extension twinning in magnesium alloys. *International Journal of Plasticity* **2018**, *106*, 186–202. doi:10.1016/j.ijplas.2018.03.008.
22. Zope, R.R.; Mishin, Y. Interatomic potentials for atomistic simulations of the Ti-Al system. *Physical Review B - Condensed Matter and Materials Physics* **2003**, *68*, 024102, [arXiv:cond-mat/0306298]. doi:10.1103/PhysRevB.68.024102.
23. Plimpton, S. Fast parallel algorithms for short-range molecular dynamics. *Journal of Computational Physics* **1995**, *117*, 1–19, [arXiv:10.1002/nag.2347]. doi:10.1006/jcph.1995.1039.
24. Hirel, P. Atomsk: A tool for manipulating and converting atomic data files. *Computer Physics Communications* **2015**, *197*, 212–219. doi:10.1016/j.cpc.2015.07.012.
25. Stukowski, A. Visualization and analysis of atomistic simulation data with OVITO—the Open Visualization Tool. *Modelling and Simulation in Materials Science and Engineering* **2010**, *18*, 015012, [arXiv:10.1002/nag.2347]. doi:10.1088/0965-0393/18/1/015012.
26. Zhu, Y.; Liao, X.; Wu, X. Deformation twinning in nanocrystalline materials. *Progress in Materials Science* **2012**, *57*, 1–62. doi:10.1016/j.pmatsci.2011.05.001.
27. Liu, Y.L.; Liu, L.M.; Wang, S.Q.; Ye, H.Q. First-principles study of shear deformation in TiAl alloys. *Journal of Alloys and Compounds* **2007**, *440*, 287–294. doi:10.1016/j.jallcom.2006.09.027.
28. Stein, D.F.; Low, J.R. Mobility of edge dislocations in silicon-iron crystals. *Journal of Applied Physics* **1960**, *31*, 362–369. doi:10.1063/1.1735574.
29. Escaig, B. L'activation thermique des déviations sous faibles contraintes dans les structures h.c. et c.c. Par. *Physica Status Solidi (B)* **1968**, *28*, 463–474. doi:10.1002/pssb.19680280203.
30. Microstructures, L. Deformation Behavior of Two-Phase  $\alpha_2$ (Ti<sub>3</sub>Al) +  $\gamma$ (TiAl) Alloys. *Gamma Titanium Aluminide Alloys* **2011**, *2*, 125–248. doi:10.1002/9783527636204.ch6.
31. Zghal, S.; Menand, A.; Couret, A. Pinning points anchoring ordinary and shockley dislocations in TiAl alloys. *Acta Materialia* **1998**, *46*, 5899–5905. doi:10.1016/S1359-6454(98)00233-X.

**Funding:** This research was funded by the National Natural Science Foundation of China (No. 51665030) and the Program for Changjiang Scholars and Innovative Research Team in Universities of the Ministry of Education of China (No. IRT-15R30) and the Doctoral Research Foundation of Lanzhou University of Technology.

© 2018 by the authors. Submitted to *Journal Not Specified* for possible open access publication under the terms and conditions of the Creative Commons Attribution (CC BY) license (<http://creativecommons.org/licenses/by/4.0/>).